Structure of Anisole Derivatives by Total Neutron and X-ray Scattering: Evidences of Weak C-H⋯O and C-H⋯π Interactions in the Liquid State.

Alessandro Triolo[1,*], Fabrizio Lo Celso[1,2], Natalia V. Plechkova[3,4], Francesca Leonelli[5], Sabrina Gärtner[6], Dean S. Keeble[7] and Olga Russina[1,5*].

[1] Laboratorio Liquidi Ionici, Istituto Struttura della Materia, Consiglio Nazionale delle Ricerche, (ISM-CNR) Rome, Italy

[2] Department of Physics and Chemistry, Università di Palermo, Palermo, Italy.

[3] Queen's University of Belfast, QUILL Research Centre, School of Chemistry & Chemical Engineering, Northern Ireland, UK

[4] Queen's University of Belfast, School of Medicine, Dentistry & Biomedical Sciences, Wellcome Wolfson Institute of Experimental Medicine, Northern Ireland, UK

[5] Department of Chemistry, University of Rome Sapienza, Rome, Italy.

[6] ISIS Facility, STFC Rutherford Appleton Laboratory, Harwell Oxford, Didcot, UK

[7] Diamond Light Source, Harwell Campus, Didcot, UK

Corresponding Authors: A. T. (triolo@ism.cnr.it); O.R. (olga.russina@uniroma1.it)

Abstract.

High resolution, total neutron and x-ray scattering data have been used in synergy with Molecular Dynamics simulations to access atomistic scale insight into the structure of anisole and 2,3,5-trimethylanisole, two aromatic compounds bearing an electron-donating methoxy group. A detailed description is provided for the main interactions occurring in these systems, including π-π stacking and weak hydrogen bonding correlations: C–H$\cdots$O and C–H$\cdots$ π. The existence of preferential orientations of the first shell coordinating molecules and the specific nature of the interactions involving the π cloud and the polar methoxy group have been reported and discussed.
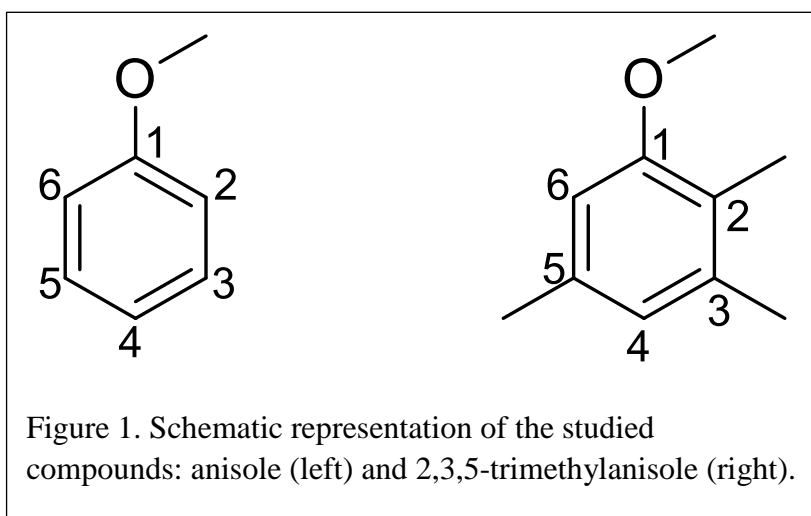
1. Introduction.

Microscopic, atomistic scale structural correlations in liquid systems are fundamental features in inducing overall macroscopic properties, such as solvation ability, that are responsible for the bulk behaviour of materials. In this context, non-covalent interactions, such as the π-π interaction that occurs between aromatic rings, attract great attention, because of their relevance in influencing the functionality of complex biological, supramolecular and petrochemical systems. These interactions are responsible for peculiar properties leading to specific structural correlations. The understanding of such effects can enable a more efficient material exploitation.

Among the most successful tools for exploring liquid structure, the joint use of X-ray/neutron scattering experiments and Molecular Dynamics (MD) simulations represents a key opportunity to access spatial correlations in amorphous systems at atomistic resolutions, thus enabling a profound understanding of the connection between the chemical properties, the resulting structural features and the eventual bulk behaviour.

This approach has become very common in the last few decades, thanks to the substantial improvement of computational tools (both hardware and software) that make statistically robust simulations achievable on a workstation within a few days. Moreover, this approach can be very powerful, especially considering the constantly growing predictive quality of existing interatomic potentials; however, a constant benchmarking of the computational output with experimentally accessible quantities is required to validate and expand the predictive ability of such simulations. In this respect, the opportunity of validating the structural properties expected as a MD output with experimentally available X-ray/neutron scattering observables is extremely valuable. These two methods are highly complementary, especially in the study of organic compounds: while X-ray radiation is more sensible to heavy atoms (e.g. carbon, oxygen), neutrons are more sensitive to hydrogen and can benefit from the selective replacement of ^1H with ^2H (deuterium).

Figure 1. Schematic representation of the studied compounds: anisole (left) and 2,3,5-trimethylanisole (right).

Here, using the approach mentioned above, two different aromatic compounds will be investigated using such an approach: methoxybenzene (anisole) and 1-methoxy-2,3,5-trimethylbenzene (2,3,5-trimethylanisole, hereinafter indicated as 3M_A) (see Figure 1).

Anisole is a feedstock compound: it is a colourless liquid with a spicy-sweet smell and it is applied as a precursor to perfumes, insect pheromones, and pharmaceuticals. The presence of the methoxy group (–O–CH$_3$) exerts an electron donor effect on the aromatic ring, thus strongly affecting the π cloud. This functionalisation allows the investigating of weak interactions, including π- π stacking and weak hydrogen bonding (HB). For the latter, the effect is not as large as in the case of phenol (where the methyl group is replaced by a hydrogen); nevertheless evidences of such interactions exist. Anisole has been studied in the past using electron diffraction[1], thus achieving information on the planarity of its heavy atom skeleton. The crystal structure has been obtained at 100 K, using single crystal X-ray diffraction,[2] confirming the planarity of the compound and highlighting the presence of an edge-to-face interaction rather than face-to-face π-π stacking. The existence of relatively short C–H$\cdots$O contacts and C–H$\cdots\pi$ system contacts has been observed.[2] Another more recent study explored the effect of external conditions to the formation of crystal phases in anisole and reported a new crystal phase obtained under high pressure conditions.[3] Also in this study, short correlations were detected between C–H and the π-system as well as C–H$\cdots$O contacts. The two phases are shown to be different in terms of packing.[2,3] Other studies focused on the rotational barrier for the rotation of the methoxy group: both theoretical[4] and experimental NMR[5] studies were reported.

3M_A is a derivate from anisole, with three methyl groups connected to the benzene ring in positions 2, 3 and 5. This compound is not as well characterised as anisole. The presence of the three methyl groups enhances electron density in the aromatic ring. Studies on related compounds 3,4 dimethylanisole[6] and 2,4 dimethylanisole[7], focused on the determination of low barriers to internal rotations of methyl groups, by microwave spectroscopy. A joint microwave spectroscopy and X-ray Diffraction study on the gas and solid state, respectively, of 2,4 dimethylanisole was also reported.[8] In the solid state, the structural study suggests the establishment of C–H$\cdots\pi$ interactions: such interactions are considered the weakest extreme of hydrogen bonds between a soft acid such as C–H and a soft base such as the π-system.[9–14] It has been reported that dispersive energy is the main contributor to C–H$\cdots\pi$ interactions, as electrostatic or charge transfer contributions are often negligible; nevertheless the dual origin (both dispersive and electrostatic) of this interaction has been stressed as the reason for the importance of this non-covalent force in chemistry and, especially, biochemistry. In the common case of aliphatic or aromatic C–H groups as hydrogen donors, the energy of a C–H$\cdots\pi$ hydrogen bond is around 2 kcal mol^{-1}.[10]

In the case of 2,4 dimethylanisole, one of the methyl groups hydrogen is pointing towards the π-system of a neighbour molecule, with a C–H$\cdots\pi$ characteristic geometry where the H$\cdots\pi$ distance is equal to ca. 3 Å and the angle C–H$\cdots\pi$ is equal to 160°.[8] A similar geometry has also been observed

in crystalline anisole (see above), although involving C–H donors belonging to methoxy methyl group.[2]

In the context of the present study, it makes sense to refer to previous structural studies on benzene that highlighted interesting features: benzene has been largely explored in the past, using synergy of X-ray and /or neutron scattering and computational tools (see e.g. [15–21]). These studies highlighted the complexity of the short-range correlations in this system in the liquid state. In particular the existence of very short range correlations (< 5 Å) between neighbouring molecules that are stacked in a parallel displaced (PD) way emerged, while face-to-face stack geometries were not found[19]. At larger correlation distances (from 5 to 7 Å), a predominance for perpendicular molecules to the reference one is found, with a preference for Y-shaped correlations, where two H atoms from the first neighbour molecule are directed towards the ring center. [19]

Overall, to our knowledge, no information is available on the structural correlations in either anisole or 3M_A in their liquid state. This study reports neutron diffraction data at ambient temperature for both compounds in their liquid state, as well as X-ray diffraction data from liquid 3M_A. These data sets have been compared with the outputs from MD simulations that were further exploited to extract atomistic level information on the structure correlations in the two compounds.

2. Experimental and Computational Part

2.1 Experimental details

Anisole and 3M_A were purchased from TCI and used as received without further treatment. The chemical structures of these compounds are shown in Figure 1.

2.1.1 X-ray scattering.

3M_A was loaded into a borosilicate capillary of 1.5 mm outer diameter, which was flame-sealed. The total high-resolution X-ray scattering data were collected on the I15-1 beamline at Diamond Light Source, UK, using x-rays of wavelength 0.161669 Å (E=76.69 keV) and a Perkin Elmer XRD 4343 CT detector. The total scattering data were integrated to 1D using DAWN[22] and then normalised and corrected to extract S(Q) using GudrunX[23,24].

2.1.2 Neutron Scattering.

The total high resolution neutron diffraction measurements on natural (*i.e.* no isotopic substitution was applied) anisole and 3M_A were performed on the SANDALS diffractometer at ISIS. The neutron wavelength range is 0.05–4.95 Å. Data was collected over the momentum transfer (Q) range between ca. 0.3 and 50 Å^{-1}. The samples were contained in chemically inert, null scattering $Ti_{0.68}Zr_{0.32}$ flat cans (with size 3.5x3.5x1 mm^3) sealed with Teflon O-rings. The scattering contributions from the container were corrected for using measurements of the empty cell. The data was normalised using measurements of a vanadium standard. Diffraction experiments were conducted at 298 K under vacuum. The diffraction patterns from the samples were measured for approximately 6 hours at full operating capacity. The data analysis was carried out using GUDRUN software[24,25] available at the facility, that allows the application of: a) normalization to the incident flux, absorption and multiple scattering corrections, empty can subtraction and normalisation to absolute units by dividing the measured differential cross section by the scattering of a vanadium standard and b) corrections for single atom scattering and hydrogen inelasticity effects.[24]

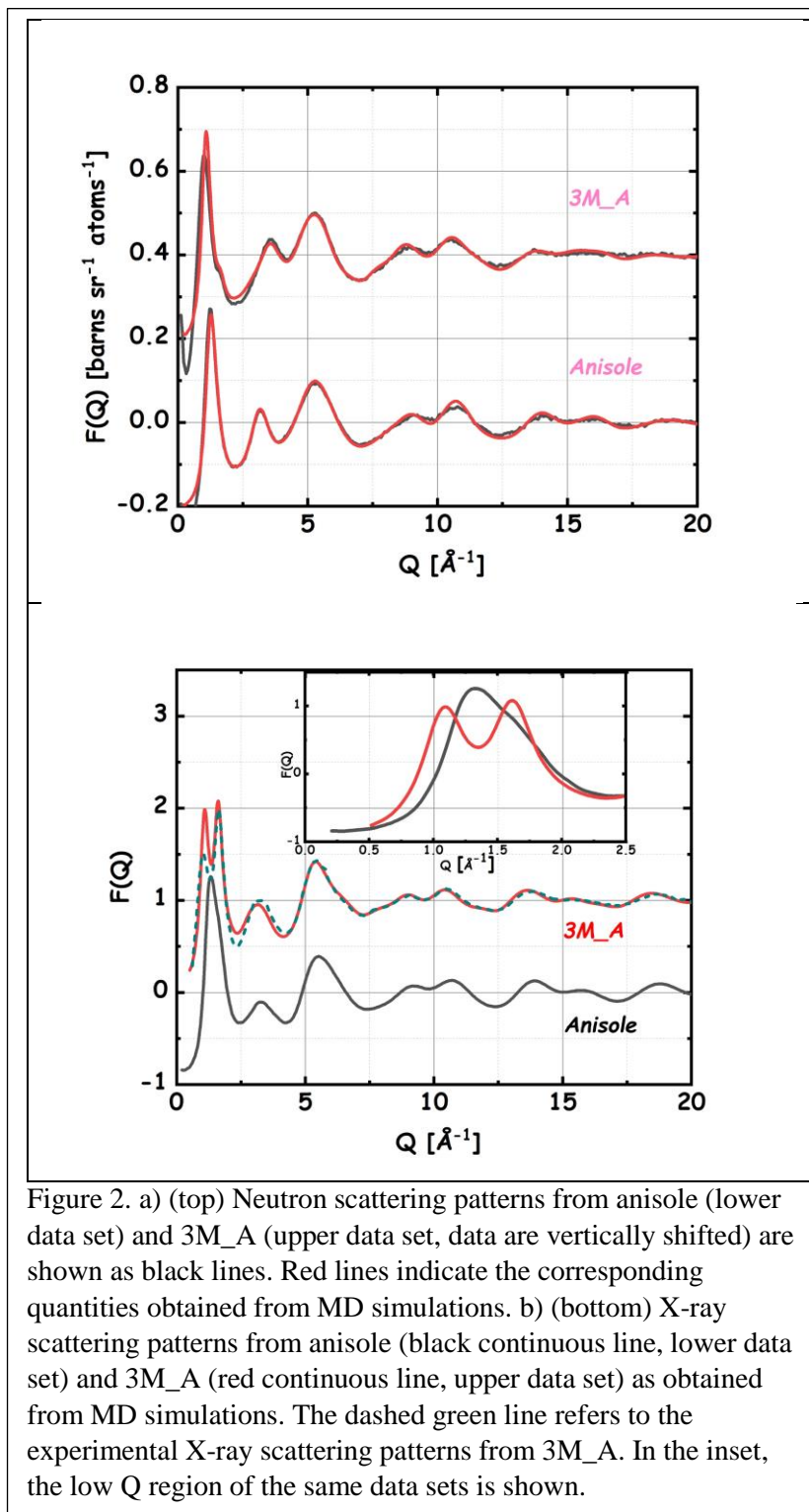### 2.2 Molecular Dynamics simulations.

Molecular dynamic simulations were performed using the GROMACS 5.1.1 package [26,27] . Bonded and non bonded parameters for the two systems, anisole and 3M_A were described using an all-

atoms potential OPLS-AA force field [28]. The simulations were performed using a cubic box of 1500 molecules; periodic boundary conditions were applied. Force field parameter files were created by DLPGEN software [29]; initial configurations were created by Packmol software [30]. The starting density was fixed 10% higher than the experimental one. The equilibration procedure was done in several steps, starting from a 5 ns NVT simulation at 400 K, followed by a series of 5 ns NPT runs lowering progressively the temperature (400 K, 350 K and then 298 K) at 1 bar. After the equilibration phase, the system was run for a total of 50 ns for a production run, and then the trajectory of the last 4 ns was saved at a frequency of 1 ps for calculation of the structural properties. The simulations were always checked versus the experimental density and the energy profile. During the production runs for the temperature coupling, we used a velocity rescaling thermostat [31] (with a time coupling constant of 0.1 ps), while for the pressure coupling, we used a Parrinello–Rahman barostat [32] (1 ps for the relaxation constant). The Leap-Frog algorithm with a 0.5 fs time step was used for integrating the equations of motion. Cut-offs for the Lennard-Jones and real space part of the Coulombic interactions were set to 11 Å. For the electrostatic interactions, the Particle Mesh Ewald (PME) summation method [33,34] was used, with an interpolation order of 6 and 0.08 nm of FFT grid spacing.

X-ray and neutron weighted structure factors were computed together with selected pair correlation functions, angular distribution functions and spatial distribution functions using TRAVIS [35–37].

3. Results and Discussion.

Anisole density has been reported in a few papers dealing with its mixtures with a variety of compounds.[38–41] Our MD computed value for this parameter at 298 K is 0.971 g/cc, which is slightly lower than the literature values (ca. -2%). The provider reports a density for compound 3M_A of 0.97 g/cc at 298 K, while our MD simulation indicates a value of 0.945 g/cc (-2.5 %).

Figure 2. a) (top) Neutron scattering patterns from anisole (lower data set) and 3M_A (upper data set, data are vertically shifted) are shown as black lines. Red lines indicate the corresponding quantities obtained from MD simulations. b) (bottom) X-ray scattering patterns from anisole (black continuous line, lower data set) and 3M_A (red continuous line, upper data set) as obtained from MD simulations. The dashed green line refers to the experimental X-ray scattering patterns from 3M_A. In the inset, the low Q region of the same data sets is shown.

Experimental Neutron (for anisole and 3M_A) and X-ray (for 3M_A) scattering patterns are reported in Figure 2 (top and bottom, respectively). In the same figures, the computed Molecular Dynamics computed scattering patterns are shown for comparison. The observed agreement between computed and experimental data sets is very good, making us confident on the quality of the chosen interaction potential for the MD simulations, to account

for structural properties of the reported compounds. The inset of Figure 2b) shows that no scattering feature can be detected for Q values lower that first peak position at ca. 1 Å^{-1}. This means that no mesoscopic organization occurs over nm spatial scale in the considered compounds, unlike other classes of compounds such as alcohols[42], dialkylsulfoxides[43], ionic

liquids[44–46] or deep eutectic solvents[47]. On the other hand, typical amorphous peaks are observed, as commonly encountered in liquid organic compounds[21] : these features correspond to intermolecular spatial correlations over scales of the order of several Å. Such spatial correlations can be better identified in the r-space domain, rather than in the Q-space. Accordingly, the forthcoming analysis will focus on the characterization of spatial correlations in terms of pair distribution functions (pdf o g_{ij}(r), indicating the normalised probability of finding a species j at a given distance, r, from the reference species i), combined distribution functions (cdf, typically reporting the combined probability of two different conditions (e.g. a distance and an angular conditions, *vide infra*)) and spatial distribution functions (sdf, describing the distribution in space (not isotropically averaged as in the case of g(r)) of a species surrounding a reference one. As was mentioned, the main computational tool used for these analysis is the TRAVIS software.[35,37]
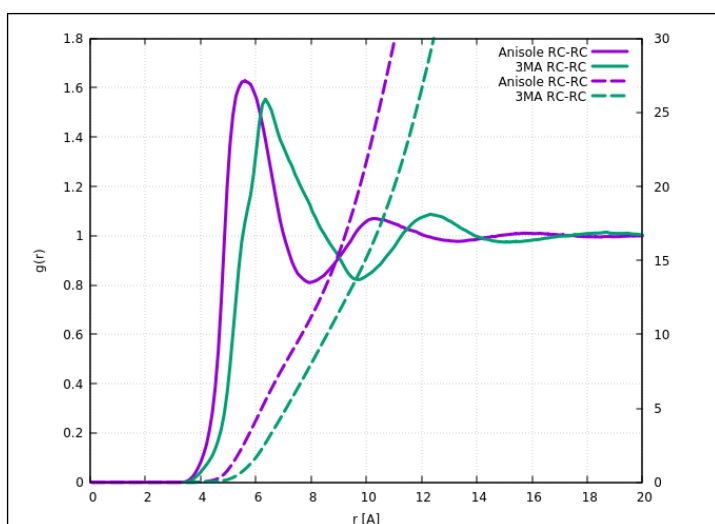

Figure 3. Pair distribution functions (continuous lines, left axis) and coordination number (dashed lines, right axis) of the rings geometrical centres of anisole (violet colour) and 3M_A (green colour), as obtained from MD simulations at 298 K.

In Figure 3, we report the pdf referring to the benzene ring's geometrical centres (RC) for the two considered compounds. We also report the integrated value of pdfs, delivering the corresponding average coordination number. It is apparent that a first solvation shell exists around a reference molecule at distances between 4 and 10 Å, depending on the considered compound. Anisole is characterised by a shorter correlation distance for this type of shell, as compared to the other bulkier compound. In particular, we find that the pdf's peaks are centred at 5.6 and 6.3 Å, for anisole and 3M_A, respectively. Integration of the mentioned pdfs up to their first minimum provides an estimate for the number of first neighbours building up the solvation shell: in its first solvation shell, anisole is surrounded by *ca.* 11 molecules, while 3M_A is surrounded by *ca.* 14 molecules. These figures are consistent with analogous findings for related aromatic and aliphatic cyclic compounds (*ca.* 13 surrounding molecules in the case of cyclohexane, methylcyclohexane, benzene and toluene[21] and ethylbenzene[48]; also Headen *et al.* report values of 12 surrounding

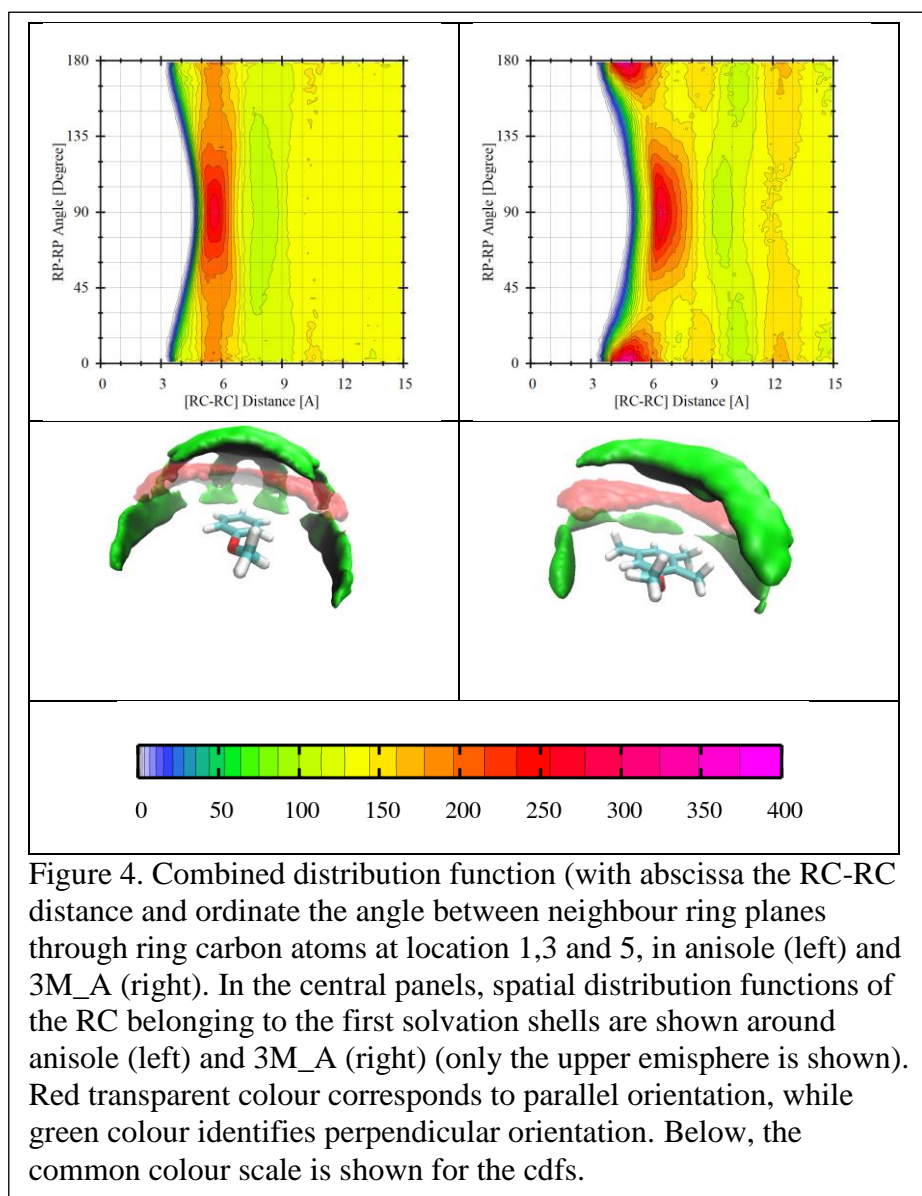molecules for both benzene and toluene[19]). The shape of the first coordination peaks reported in Figure 3 suggests a complex organization of first neighbours belonging to the shell. In order to rationalise this hypothesis, in Figure 4 we report the cdf's reflecting the orientation of neighbour molecules ring plane (RP) with respect to the reference one (angle θ between the lines perpendicular to these planes), as a function of RC-RC distance. A somehow different behaviour is observed for the two compounds, anisole and 3M_A, which are characterised by the presence of surrounding molecules already at

Figure 4. Combined distribution function (with abscissa the RC-RC distance and ordinate the angle between neighbour ring planes through ring carbon atoms at location 1,3 and 5, in anisole (left) and 3M_A (right). In the central panels, spatial distribution functions of the RC belonging to the first solvation shells are shown around anisole (left) and 3M_A (right) (only the upper emisphere is shown). Red transparent colour corresponds to parallel orientation, while green colour identifies perpendicular orientation. Below, the common colour scale is shown for the cdfs.

distances as short as 3.5 Å. However, it appears that the surrounding molecules show different preferential orientation with respect to the reference one, in the solvation shell between 4 and 8 Å. The most preferred configuration of neighbour anisole molecules is perpendicular ($60°<θ<120°$) and they are distributed at a distance between 5 and 6 Å from the reference molecule; however, a more limited yet non-negligible population of parallel molecules ($0°<θ<15°$ and $165°<θ<180°$) exists at even shorter distances ($4<r$ (Å)<5). On the other hand the situation for 3M_A is different: the most preferred distribution is with parallel molecules at shorter distances ($4<r$ (Å)<6), while at larger distances ($6<r$ (Å)<8), the molecules organise themselves perpendicularly to the reference. This situation can be further understood by inspection of the spatial distribution function of RCs around reference molecules. In Figure 4 (central panels), we separately report the distributions of RC belonging to either parallel (transparent red colour lobes) or perpendicularly (green lobes)

oriented molecules. The closest approach is achieved by parallel molecules: in both compounds, they organise in a Parallel Displacement fashion above and below the reference molecule plane. Perpendicularly oriented molecules are localised further apart both below and above the reference molecules. Moreover, while in the case of anisole, the lantern-like distribution is observed (at least around the portion of the aromatic ring far from the methoxy group), with lobes directed towards the centre of the aromatic C–C bond, in the case of 3M_A, such distribution is not observed and one rather finds equatorially distributed molecules, in order to ensure contacts with methyl groups or aromatic hydrogens. An indication of interaction of perpendicularly oriented molecules with the methoxy group is also found.

This organization is quite similar to the one reported for benzene and toluene (and analogous derivated benzenes), where short distance parallelism and larger distance perpendicular organization (yet with some parallel component) were observed.[19,21,48]
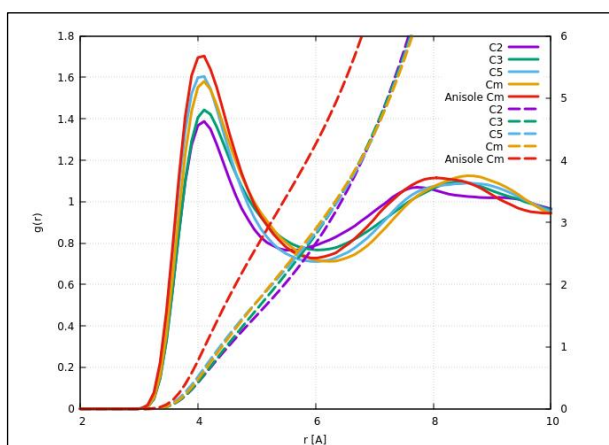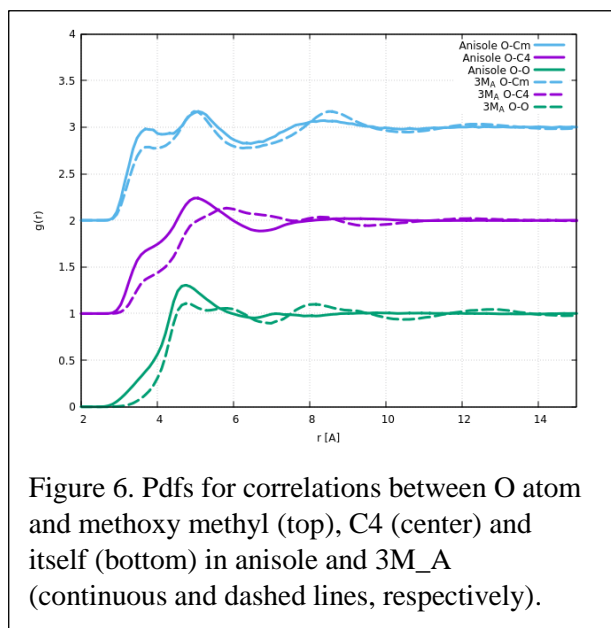

Figure 5. Pdfs (continuous lines, left axis) and corresponding coordination number (dashed lines, right axis) for methyl group correlations in anisole and 3M_A.

The structural organisation between neighbour molecules can be influenced also by other effects. The presence of methyl groups in both anisole and 3M_A might induce the tendency of these groups to cluster, due to dispersive interactions. In Figure 5, we show the pdfs and the corresponding coordination numbers for each methyl group (MG) with any other MG (in the case of anisole only the methoxy MG is considered; for 3M_A all the MGs are considered). It emerges that a main correlation peak is invariably located at *ca.* 4.1 Å. The coordination numbers sum up to *ca.* 4 for anisole and between 2 and 3 for 3M_A. The corresponding pdf has been reported for methyl groups in toluene: Headen *et al.* report a peak centred at 4.15 Å with amplitude *ca.* 1.6 and a number of neighbours equals to 1.5 (for the solvation shell extending up to 4.5 Å[19]: we notice that we integrated the pdf peak up to its minimum, *i.e.* 5.5. and 6 Å, for anisole and 3M_A, respectively, so a comparison is not possible). Our current estimate suggests that in the case of anisole, there might be a more specific methyl-methyl interaction, rather than a mere steric induced effect; however, such effect does not seem to be appreciable in the case of 3M_A.
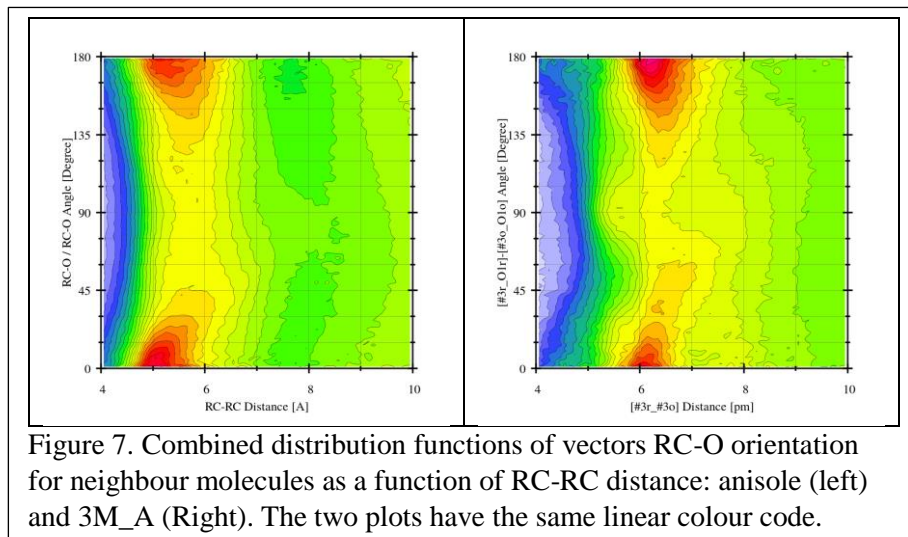
The polar nature of the oxygen atom belonging to the methoxy group might also induce effects on the local ordering, as well. In Figure 6, we report the pdfs of O with the methoxy methyl group (Cm), the C atom in position 4 and itself. Overall, we observe a more extended range of correlations in 3M_A than in anisole, as indicated by the existence of oscillations in 3M_A patterns at larger distances than in anisole. The pdf between O and Cm shows two short range peaks at 3.7 and 5.1 Å, similar to observations by Jorgensen *et al.* for dimethyl ether[49]. The same authors mentioned O-O correlations with a minimum approach distance of ca. 3.5 Å. While the same is true for 3M_A, in the

Figure 6. Pdfs for correlations between O atom and methoxy methyl (top), C4 (center) and itself (bottom) in anisole and 3M_A (continuous and dashed lines, respectively).

case of anisole, a closer approach is possible already at distances as short as 2.8 Å, with a total of 5.5 neighbour O's surrounding the reference one in its first solvation shell (r<6.5 Å). Overall, however, peaks are large and weak, as expected for weakly correlated systems.

In Figures 7, we show the cdfs related to the mutual orientation of the vectors connecting the RC and the O atom in neighbour molecules (θ), as a function of RC-RC distance. It appears that while in anisole a slight preference is expressed for parallel alignment ($\theta \sim 0°$), with shorter approach distance and narrower angular distribution than the

Figure 7. Combined distribution functions of vectors RC-O orientation for neighbour molecules as a function of RC-RC distance: anisole (left) and 3M_A (Right). The two plots have the same linear colour code.

antiparallel alignment, in the case of 3M_A, a clear preference is expressed for anti-parallel alignment ($\theta \sim 180°$), although with a more heterogeneous distribution (both in terms of distance and angular distributions).

In order to better visualise the nature of interactions between neighbour molecules, we also

Figure 8. Spatial distribution of oxygen atom surrounding reference anisole and 3M_A compounds. (Left) Pair distribution function and coordination numbers of RC-O correlations for the two compounds. Spatial distribution function of oxygen atom surrounding reference anisole (center) and 3M_A (right). Distribution isovalues refer approximately to half of the maximum amplitude. a) anisole, red (layer between 0 and 5.5 Å), transparent yellow (layer between 5.5 and 7.4 Å); b) 3M_A, red (layer between 0 and 5.5 Å), transparent yellow (layer between 5.5 and 9.2 Å).

explored the distribution of oxygen atoms around the references molecules. In Figure 8, the pdfs and the coordination numbers between RC and O atoms are shown. Anisole's O approaches the reference closer than in the case of 3M_A, with a peak centred at *ca.* 5 Å. 3M_A's pdf shows a main peak at 6 Å and the latter has a shoulder centred at 5 Å. Furthermore, both anisole and 3M_A show a complex peak shape, indicating the coexistence of different local environment of O solvation around the reference molecule. Overall *ca.* 8 and 11 O atoms build up the first solvation shell in anisole and 3M_A, respectively. Spatial distribution functions can be of help in rationalising this organization; in particular, we evaluated O sdfs for RC–O ranges: a) 0 - 5.5 Å and b) 5.5 - 7.4/9.2 Å, as 5.5 Å seems to indicate the upper border for a specific solvation, while 7.4 and 9.2 Å are the upper borders of the first solvation shell for anisole and 3M_A, respectively. These sdfs are shown in Figure 8. In the case of anisole, the first layer (a) is composed by O atoms lying on top and bottom of the reference ring, as well as, forming six equatorial lobes directed towards C–C aromatic bonds (thus, prompting for bifurcated HB). Moreover, there is a distinct O atoms ring distribution surrounding the location of methoxymethyl group. The outer layer (b) has no top and bottom component; it forms lantern-like distributions at larger distances than the equatorial lobes and extends the distribution surrounding the methyl group.

In the case of 3M_A, the two distributions are analogous to the case of anisole, with top and bottom distributions, as well as, four equatorial lobes directed towards C–C aromatic bonds; the distribution surrounding the methoxy group occurs at larger distances and there are two further long distance (ca. 8.5 Å) lobes localised above and below the reference plane. The lantern-like distribution with four branches is localised between methyl groups, but it is not as well defined as in the case of anisole.

The methoxy group has been recognised as a hydrogen bonding acceptor in several crystalline structures.[50] The X–H⋯O bond between different species (e.g. HF, H_2O, NH_2CH_3, etc.) and the methoxy's oxygen atoms has been identified and considered important for solid-state structural organization. It makes sense to explore the nature of $C_{aromatic}$–H⋯O and $C_{aliphatic}$–H⋯O correlations in the presently considered compounds. Figure 9 shows H⋯O pdfs for selected pairs in anisole and 3M_A. In all the mentioned cases, the short distance peaks, centred at *ca.* 3 Å, are characterised by
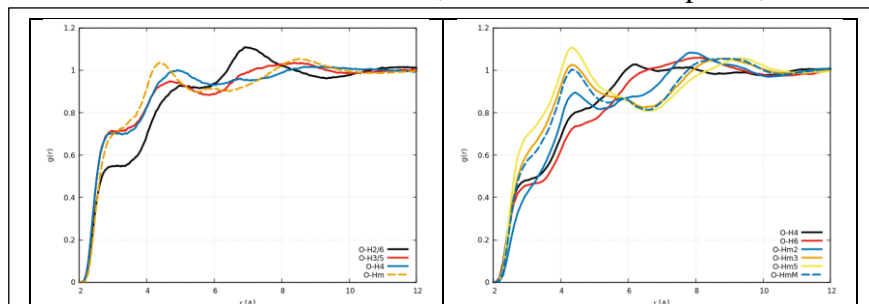
Figure 9. Pdfs related to correlations between methoxy O and different H belonging to the ring or the methyl groups in anisole (left) and 3M_A (right).

a low amplitude, substantially below unity, which would indicate bulk average correlation. Accordingly, these are not common interactions in these systems. Nevertheless, considering the typical weakness of interactions occurring in these compounds, it makes sense to further explore the nature of such structural correlations.

By pdfs integration up to 3.5 Å, the number of neighbour contacts has been estimated and the average number of oxygen atoms surrounding each hydrogen atoms belonging either to the ring or to the methyl groups varies between 0.2 and 0.5.

The combined distribution functions, joining distance and angular conditions for these weak correlations have been computed and selected patterns for the aromatic H6 are shown in Figure 10
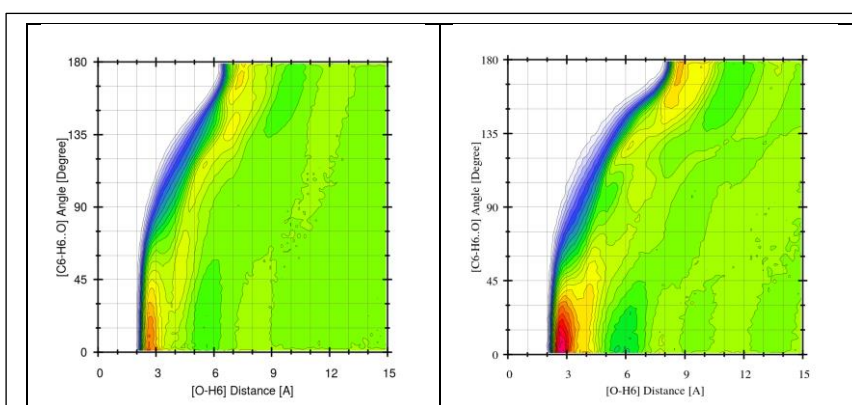

Figure 10. Selected cdfs referring to H atom in position 6 and its correlation with the methoxy O in anisole (left) and 3M_A (right) (same colour map was used).

(all the cdfs are reported in the Supplementary Information), for both anisole and 3M_A. In general, in anisole, H's in positions 2 and 6 are coordinated by O's at distances < 3 Å and the angle C–H⋅⋅O is <30°. A similar behaviour is found for H's belonging to the methoxymethyl, although the corresponding peak is smaller in amplitude. H's in positions 3-5 are characterised by H⋅⋅O distances < 3 Å, but the angle C–H⋅⋅O extends up to 75°. In 3M_A, only Hs in position 4 and 6 are characterised by an intense peak corresponding to H⋅⋅O distances < 3 Å and C–H⋅⋅O angles <45°.

H· ·O correlations involving Hs belonging to methyl groups are characterised by weaker lobes with H· ·O distances ≥ 3 Å and C–H· ·O angles that can extend above 45°.

On average, the total number of H atoms belonging to the considered compounds is surrounded (by a distance < 3.5 Å) by the same amount of methoxy Os, namely, *ca.* 3.5. Considering, however, the different number of Hs belonging to the compounds the coordination of the average molecule by O atoms follows the order anisole>3M_A.

Another potential interaction taking place in the considered compounds is the C–H···π one. This is known to play a role on crystalline states of matter and therefore, can play a role in orienting correlations also in the liquid state, when there are no other strong interactions taking place that might overcome such a role, (we remind that it belongs to the weakest extreme of hydrogen bonds, between a soft acid C–H and a soft base π-system)[51]. Typical geometric parameters for C–H···π HBs in the solid state are: RC···H distance ~ 2.6-2.8 Å and C–H···RC angle ~ 150-160°.[51] In the liquid state, one can expect these parameters to be more relaxed. In Figure 11, we show pdfs for H atom in position 6 with respect to the RC of anisole and 3M_A, differentiating the two cases of the vector RC···H making an angle with the line perpendicular to the ring plane between 0 and 10 ° (dashed lines) and between 80 and 90° (continuous lines): *i.e.* orthogonal and equatorial H positions with respect to the molecule plane, respectively.
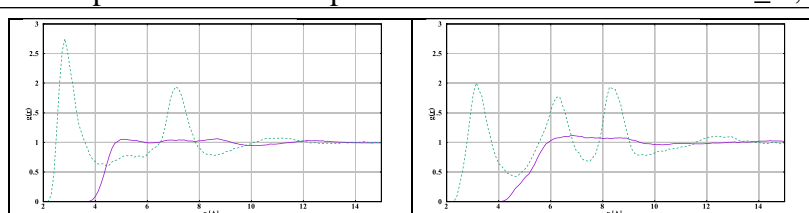

Figure 11. Pdfs referring to H atom in position 6 and its correlation with the Ring Center in anisole (left) and 3M_A (right). Differentiation is shown for H atoms lying above/below (0°, dashed line) or equatorially (90°, continuous line) to the Ring.

It clearly emerges that both aromatic compounds are characterised by a distinct anisotropy in the distribution of the H atoms closely surrounding the reference ring. The characteristic distance of the first neighbour to the RC is of the order of 3 Å for both anisole and 3M_A. Such a short distance population is detectable only in the case of linear C–H···π organization (that means for molecules lying above/below the reference molecule plane), while equatorial distribution of H atoms does not show indication of specific correlation at short distance. Accordingly, while the parallel organization of molecules (accounted for in Figure 4) leads to the closest approach, it is only the perpendicular organization that can lead to the development of $C_{aromatic}$–H···π correlations. These results are evidences for the existence of long but not negligible C–H···π coordination in the probed aromatic compounds. This description is quite general. In the Supplementary Information, we report the cdfs corresponding to the C–H···π structural organization for all the possible C-H moieties. One can generalise those figures in the following terms:

- anisole. All the shortest H⋯π distances are between 3 and 4 Å, with the angle C–H⋯π having a broad distribution between 0 and 90°. We notice that also the methyl group Hs are involved in the C–H⋯π interaction.

- 3M_A. Similarly to anisole, the shortest H⋯π distances are between 3 and 4 Å, however, notably, the angle C–H⋯π is characterised by a much narrower distribution between 0 and 45°. An inspection of sdf's (data not shown) for both anisole and 3M_A shows that the hottest distribution lobe for any H atoms, at distances below 4 Å from the RC, is due to molecules located above and below the ring plane.

It is noteworthy that crystallographic publications on anisole report the existence of short H⋯O and H⋯π distances of the order of 2.7-2.9 Å at low temperature/high pressure. [2,3] Such short correlations correspond to the ones found in the liquid state at *ca.* 2.5-3.0 Å and 3.0-4.0 Å, respectively, in the previous discussion.

4. Conclusion.

We explored the structural properties of anisole and 2,3,5-trimethylanisole (3M_A) using a synergy of experimental and computational tools. We reported original total high resolution neutron scattering data sets for both compounds and X-ray data set for 3M_A. Molecular Dynamics simulations, using an all-atom non-polarizable potential, were developed for the first time for these aromatic compounds, in order to access structural features of their short-medium range order at atomistic scale. The computed neutron and X-ray diffraction patterns are in very good agreement with the experimental data sets, thus providing a robust validation of the structural information extracted by the mentioned simulations.

Anisole and 3M_A are surrounded by a first solvating shell of 11 and 14 neighbours, respectively. Such a solvation shell appears to be heterogeneous in terms of both its spatial distribution around the reference molecule and the local orientation of each of the constituent molecules. Similarly to previous studies on other aromatic simple molecules, the closest molecules are organised with a parallel orientation to the reference, while molecules at a larger distance (but still belonging to the first solvation shell) are perpendicular to the central one. In the case of 3M_A, the first population is more populated than in the case of anisole. These two populations are spatially distributed in different ways: the closely approaching parallel molecules are localised above and below the reference molecule in a parallel-displaced stack way. The perpendicularly oriented molecules are also distributed in these locations, though at a higher distance, but they also form a characteristic lantern-like or equatorial distribution, for anisole and 3M_A, respectively, thus prompting for Y-shaped correlations between neighbouring molecules. In 3M_A, evidences of correlations with the methoxy methyl group are also found. Both lantern and equatorial distributions are localised in such a way as to enable interactions with the group pair (either H or $-CH_3$) linked to a C–C aromatic bond. We further explored other potential interactions taking place in these systems: the occurrence of hydrophobic methyl-methyl (MG-MG) correlations and O driven interactions were probed. A distance of closest approach of ca. 4 Å was found for MG-MG with a number of neighbours of 4 and ca. 2.5 for anisole and 3M_A, respectively, prompting for potential specific interaction in the case of anisole. Weak O-mediated interactions were found, similarly to the case of dimethylether. Oxygen is however responsible for privileged interactions with hydrogen atoms belonging either to the aromatic ring or to the MG's. O's lantern-like or equatorial distributions were observed around central molecules, suggesting the existence of bifurcated O$\cdots$H bonds. O$\cdots$H interactions were found to be characterised by distances of the order of < 3 Å, with C–H$\cdot\cdot$O angles between 0-45° and 0-30° for anisole and 3M_A, respectively. Finally, we investigated the existence of C–H$\cdots\pi$ interactions: we observed that the distance of closest approach between H and the π system (ca. 3

Å) is achieved for nearly linear C–H$\cdots\pi$ distribution. When departing from such linearity, close contact is no longer possible. This implies that only orthogonal molecules to the reference molecular plane can establish such interactions that, accordingly, involves the perpendicularly oriented molecules lying above and below the reference plane. We observed a higher degree of linearity in the case of 3M_A than in anisole, presumably due either to steric requirements or to the electron-donating role played by methyl groups that enhances the electron distribution in the π cloud.

Overall, this study provides an accurate atomistic description of the complex interplay of steric and electrostatic interactions driving the morphology of these aromatic compounds. The presence of weak, though appreciable, C–H$\cdot\cdot$O and C–H$\cdots\pi$ interactions in the liquid state is established and can provide a useful guide to analyse and interpret related compounds. The competition of these interactions with analogues arising in binary mixtures with alcohols and water is currently under investigation and will be reported subsequently.

5. Acknowledgements.

Bibliography

(1)   Seip, H. M.; Seip, R. On the Structure of Gaseous Anisole. *Acta Chem. Scand.* **1973**, *27* (November), 4024–4027. https://doi.org/10.3891/acta.chem.scand.27-4024.

(2)   Seidel, R. W.; Goddard, R. Anisole at 100 K: The First Crystal Structure Determination. *Acta Crystallogr. Sect. C Struct. Chem.* **2015**, *71* (I), 664–666. https://doi.org/10.1107/S2053229615012553.

(3)   Smith, E. L.; Ridout, J.; Sellars, J. D.; Probert, M. R. A Structural Exploration of Anisole Accessed through Extreme Crystallisation Conditions. *CrystEngComm* **2019**, *21* (30), 4422–4426. https://doi.org/10.1039/c9ce00870e.

(4)   Spellmeyer, D. C.; Grootenhuis, P. D. J.; Miller, M. D.; Kuyper, L. F.; Kollman, P. A. Theoretical Investigations of the Rotational Barrier in Anisole: An Ab Initio and Molecular Dynamics Study. *J. Phys. Chem.* **1990**, *94* (11), 4483–4491. https://doi.org/10.1021/j100374a026.

(5)   Celebre, G.; De Luca, G.; Longeri, M.; Emsley, J. W. Internal Rotation Potential Function for Anisole in Solution: A Liquid Crystal NMR Study. *J. Phys. Chem.* **1992**, *96* (6), 2466–2470. https://doi.org/10.1021/j100185a015.

(6)   Ferres, L.; Cheung, J.; Stahl, W.; Nguyen, H. V. L. Conformational Effect on the Large Amplitude Motions of 3,4-Dimethylanisole Explored by Microwave Spectroscopy. *J. Phys. Chem. A* **2019**, *123* (16), 3497–3503. https://doi.org/10.1021/acs.jpca.9b00029.

(7)   Ferres, L.; Stahl, W.; Nguyen, H. V. L. Low Torsional Barrier Challenges in the Microwave Spectrum of 2,4-Dimethylanisole. *J. Chem. Phys.* **2019**, *151* (10), 104310. https://doi.org/10.1063/1.5116304.

(8)   Ferres, L.; Truong, K.; Stahl, W.; Nguyen, H. V. L. Interplay Between Microwave Spectroscopy and X-ray Diffraction: The Molecular Structure and Large Amplitude Motions of 2,3-Dimethylanisole. *ChemPhysChem* **2018**, *19* (14), 1781–1788. https://doi.org/10.1002/cphc.201800115.

(9)   Nishio, M.; Umezawa, Y.; Fantini, J.; Weiss, M. S.; Chakrabarti, P. CH-π Hydrogen Bonds in Biological Macromolecules. *Phys. Chem. Chem. Phys.* **2014**, *16* (25), 12648–12683. https://doi.org/10.1039/c4cp00099d.

(10)   Takahashi, O.; Kohno, Y.; Nishio, M. Relevance of Weak Hydrogen Bonds in the Conformation of Organic Compounds and Bioconjugates: Evidence from Recent Experimental Data and High-Level Ab Initio MO Calculations. *Chem. Rev.* **2010**, *110* (10), 6049–6076. https://doi.org/10.1021/cr100072x.

(11)   Nishio, M. The CH/π Hydrogen Bond in Chemistry. Conformation, Supramolecules, Optical Resolution and Interactions Involving Carbohydrates. *Phys. Chem. Chem. Phys.* **2011**, *13* (31), 13873–13900. https://doi.org/10.1039/c1cp20404a.

(12) Nishio, M. CH/π Hydrogen Bonds in Crystals. *CrystEngComm* **2004**, *6*, 130–158. https://doi.org/10.1039/b313104a.

(13) Takahashi, O.; Kolno, Y.; Iwasaki, S.; Saito, K.; Iwaoka, M.; Tomoda, S.; Umezawa, Y.; Tsuboyama, S.; Nishio, M. Hydrogen-Bond-like Nature of the CH/π Interaction as Evidenced by Crystallographic Database Analyses and Ab Initio Molecular Orbital Calculations. *Bull. Chem. Soc. Jpn.* **2001**, *74* (12), 2421–2430. https://doi.org/10.1246/bcsj.74.2421.

(14) Tsuzuki, S. CH/π Interactions. *Annu. Reports Prog. Chem. - Sect. C* **2012**, *108*, 69–95. https://doi.org/10.1039/c2pc90003c.

(15) Katzoff, S. X-Ray Studies of the Molecular Arrangement in Liquids. *J. Chem. Phys.* **1934**, *2* (12), 841–851. https://doi.org/10.1063/1.1749406.

(16) Narten, A. H. Diffraction Pattern and Structure of Liquid Benzene. *J. Chem. Phys.* **1968**, *48* (4), 1630–1634. https://doi.org/10.1063/1.1668888.

(17) Narten, A. H. X-Ray Diffraction Pattern and Models of Liquid Benzene. *J. Chem. Phys.* **1977**, *67* (5), 2102. https://doi.org/10.1063/1.435096.

(18) Tassaing, T.; Cabaço, M. I.; Danten, Y.; Besnard, M. The Structure of Liquid and Supercritical Benzene as Studied by Neutron Diffraction and Molecular Dynamics. *J. Chem. Phys.* **2000**, *113* (9), 3757–3765. https://doi.org/10.1063/1.1287787.

(19) Headen, T. F.; Howard, C. A.; Skipper, N. T.; Wilkinson, M. A.; Bowron, D. T.; Soper, A. K. Structure of π - π Interactions in Aromatic Liquids. **2010**, No. Figure 1, 5735–5742.

(20) Katayama, M.; Ashiki, S.; Amakasu, T.; Ozutsumi, K. Liquid Structure of Benzene and Its Derivatives as Studied by Means of X-Ray Scattering. *Phys. Chem. Liq.* **2010**, *48* (6), 797–809. https://doi.org/10.1080/00319104.2010.483529.

(21) Falkowska, M.; Bowron, D. T.; Manyar, H. G.; Hardacre, C.; Youngs, T. G. A. Neutron Scattering of Aromatic and Aliphatic Liquids. *ChemPhysChem* **2016**, *17* (13), 2043–2055. https://doi.org/10.1002/cphc.201600149.

(22) Filik, J.; Ashton, A. W.; Chang, P. C. Y.; Chater, P. A.; Day, S. J.; Drakopoulos, M.; Gerring, M. W.; Hart, M. L.; Magdysyuk, O. V.; Michalik, S.; et al. Processing Two-Dimensional X-Ray Diffraction and Small-Angle Scattering Data in DAWN 2. *J. Appl. Crystallogr.* **2017**, *50* (3), 959–966. https://doi.org/10.1107/S1600576717004708.

(23) Soper, A. K.; Barney, E. R. Extracting the Pair Distribution Function from White-Beam X-Ray Total Scattering Data. *J. Appl. Crystallogr.* **2011**, *44* (4), 714–726. https://doi.org/10.1107/S0021889811021455.

(24) Soper, A. K. The Radial Distribution Functions of Water as Derived from Radiation Total Scattering Experiments: Is There Anything We Can Say for Sure? *ISRN Phys. Chem.* **2013**, *2013*, 1–67. https://doi.org/10.1155/2013/279463.

(25) Soper, A. K. Computer Simulation as a Tool for the Interpretation of Total Scattering Data from Glasses and Liquids. *Mol. Simul.* **2012**, *38* (14–15), 1171–1185. https://doi.org/10.1080/08927022.2012.732222.

(26) Hess, B.; Kutzner, C.; van der Spoel, D.; Lindahl, E. GROMACS 4: Algorithms for Highly Efficient, Load-Balanced, and Scalable Molecular Simulation. *J. Chem. Theory Comput.* **2008**, *4* (3), 435–447. https://doi.org/10.1021/ct700301q.

(27) Van Der Spoel, D.; Lindahl, E.; Hess, B.; Groenhof, G.; Mark, A. E.; Berendsen, H. J. C. GROMACS: Fast, Flexible, and Free. *J. Comput. Chem.* **2005**, *26* (16), 1701–1718.

https://doi.org/10.1002/jcc.20291.

(28) Jorgensen, W. L.; Maxwell, D. S.; Tirado-rives, J.; Haven, N. Development and Testing of the OPLS All-Atom Force Field on Conformational Energetics and Properties of Organic Liquids. **1996**, *118* (45), 11225–11236. https://doi.org/10.1021/ja9621760.

(29) Bernardes, C. E. S.; Joseph, A. Evaluation of the OPLS-AA Force Field for the Study of Structural and Energetic Aspects of Molecular Organic Crystals. *J. Phys. Chem. A* **2015**, *119* (12), 3023–3034. https://doi.org/10.1021/jp512349r.

(30) Martínez, L.; Andrade, R.; Birgin, E. G.; Martínez, J. M. PACKMOL: A Package for Building Initial Configurations for Molecular Dynamics Simulations. *J. Comput. Chem.* **2009**, *30* (13), 2157–2164. https://doi.org/10.1002/jcc.21224.

(31) Bussi, G.; Donadio, D.; Parrinello, M. Canonical Sampling through Velocity Rescaling. *J. Chem. Phys.* **2007**, *126* (1), 014101. https://doi.org/10.1063/1.2408420.

(32) Parrinello, M.; Rahman, A. Polymorphic Transitions in Single Crystals: A New Molecular Dynamics Method. *J. Appl. Phys.* **1981**, *52* (12), 7182–7190. https://doi.org/10.1063/1.328693.

(33) Darden, T.; York, D.; Pedersen, L. Particle Mesh Ewald: An N·log(N) Method for Ewald Sums in Large Systems. *J. Chem. Phys.* **1993**, *98* (12), 10089–10092. https://doi.org/10.1063/1.464397.

(34) Essmann, U.; Perera, L.; Berkowitz, M. L.; Darden, T.; Lee, H.; Pedersen, L. G. A Smooth Particle Mesh Ewald Method. *J. Chem. Phys.* **1995**, *103* (19), 8577–8593. https://doi.org/10.1063/1.470117.

(35) Brehm, M.; Kirchner, B. TRAVIS - A Free Analyzer and Visualizer for Monte Carlo and Molecular Dynamics Trajectories. *J. Chem. Inf. Model.* **2011**, *51* (8), 2007–2023. https://doi.org/10.1021/ci200217w.

(36) Hollóczki, O.; Macchiagodena, M.; Weber, H.; Thomas, M.; Brehm, M.; Stark, A.; Russina, O.; Triolo, A.; Kirchner, B. Triphilic Ionic-Liquid Mixtures: Fluorinated and Non-Fluorinated Aprotic Ionic-Liquid Mixtures. *ChemPhysChem* **2015**, *16* (15), 3325–3333. https://doi.org/10.1002/cphc.201500473.

(37) Brehm, M.; Thomas, M.; Gehrke, S.; Kirchner, B. TRAVIS—A Free Analyzer for Trajectories from Molecular Simulation. *J. Chem. Phys.* **2020**, *152* (16), 164105. https://doi.org/10.1063/5.0005078.

(38) Baragi, J. G.; Aralaguppi, M. I.; Aminabhavi, T. M.; Kariduraganavar, M. Y.; Kittur, A. S. Density, Viscosity, Refractive Index, and Speed of Sound for Binary Mixtures of Anisole with 2-Chloroethanol, 1,4-Dioxane, Tetrachloroethylene, Tetrachloroethane, DMF, DMSO, and Diethyl Oxalate at (298.15, 303.15, and 308.15) K. *J. Chem. Eng. Data* **2005**, *50* (3), 910–916. https://doi.org/10.1021/je049610v.

(39) Bhumkar, A. N.; Rathnam, M. V. Density, Viscosity, and Speed of Sound of Binary Liquid Mixtures of Vinyl Acetate with Butyl Vinyl Ether, Diisopropyl Ether, Anisole and Dibutyl Ether. *J. Chem. Thermodyn.* **2019**, *136*, 77–87. https://doi.org/10.1016/j.jct.2019.04.018.

(40) Rathnam, M. V.; Ambavadekar, D. R.; Nandini, M. Densities, Viscosities, and Sound Speed of Binary Mixtures of Hexyl Acetate with Tetrahydrofuran, 1,4-Dioxane, Anisole, and Butyl Vinyl Ether. *J. Chem. Eng. Data* **2013**, *58* (12), 3370–3377. https://doi.org/10.1021/je400539h.

(41) Al-Kandary, J. A.; Al-Jimaz, A. S.; Abdul-Latif, A. H. M. Viscosities, Densities, and Speeds of Sound of Binary Mixtures of Benzene, Toluene, o-Xylene, m-Xylene, p-Xylene, and Mesitylene with Anisole at (288.15, 293.15, 298.15, and 303.15) K. *J. Chem. Eng. Data* **2006**, *51* (6), 2074–2082. https://doi.org/10.1021/je060170c.

(42) Tomšič, M.; Jamnik, A.; Fritz-Popovski, G.; Glatter, O.; Vlček, L. Structural Properties of Pure Simple Alcohols from Ethanol, Propanol, Butanol, Pentanol, to Hexanol: Comparing Monte Carlo Simulations with Experimental SAXS Data. *J. Phys. Chem. B* **2007**, *111* (7), 1738–1751. https://doi.org/10.1021/jp066139z.

(43) Lo Celso, F.; Aoun, B.; Triolo, A.; Russina, O. Liquid Structure of Dibutyl Sulfoxide. *Phys. Chem. Chem. Phys.* **2016**, *18* (23), 15980–15987. https://doi.org/10.1039/c6cp02335e.

(44) Triolo, A.; Russina, O.; Bleif, H. J.; Di Cola, E. Nanoscale Segregation in Room Temperature Ionic Liquids. *J. Phys. Chem. B* **2007**, *111* (18), 4641–4644. https://doi.org/10.1021/jp067705t.

(45) Russina, O.; Triolo, A.; Gontrani, L.; Caminiti, R. Mesoscopic Structural Heterogeneities in Room-Temperature Ionic Liquids. *J. Phys. Chem. Lett.* **2012**, *3* (1), 27–33. https://doi.org/10.1021/jz201349z.

(46) Russina, O.; Lo Celso, F.; Plechkova, N. V.; Triolo, A. Emerging Evidences of Mesoscopic-Scale Complexity in Neat Ionic Liquids and Their Mixtures. *J. Phys. Chem. Lett.* **2017**, *8* (6), 1197–1204. https://doi.org/10.1021/acs.jpclett.6b02811.

(47) McDonald, S.; Murphy, T.; Imberti, S.; Warr, G. G.; Atkin, R. Amphiphilically Nanostructured Deep Eutectic Solvents. *J. Phys. Chem. Lett.* **2018**, *9* (14), 3922–3927. https://doi.org/10.1021/acs.jpclett.8b01720.

(48) Szala-Bilnik, J.; Falkowska, M.; Bowron, D. T.; Hardacre, C.; Youngs, T. G. A. The Structure of Ethylbenzene, Styrene and Phenylacetylene Determined by Total Neutron Scattering. *ChemPhysChem* **2017**, *18* (18), 2541–2548. https://doi.org/10.1002/cphc.201700393.

(49) Jorgensen, W. L.; Ibrahim, M. Structures and Properties of Organic Liquids: N-Alkyl Ethers and Their Conformational Equilibria. *J. Am. Chem. Soc.* **1981**, *103* (14), 3976–3985. https://doi.org/10.1021/ja00404a003.

(50) Palusiak, M.; Grabowski, S. J. Methoxy Group as an Acceptor of Proton in Hydrogen Bonds. *J. Mol. Struct.* **2002**, *642* (1–3), 97–104. https://doi.org/10.1016/S0022-2860(02)00406-4.

(51) Nishio, M. The CH/π Hydrogen Bond: Implication in Chemistry. *J. Mol. Struct.* **2012**, *1018*, 2–7. https://doi.org/10.1016/j.molstruc.2012.03.012.